Radiochim. Acta **101**, 211–219 (2013) / **DOI** 10.1524/ract.2013.2027

Prediction of the thermal release of transactinide elements ($112 \leq Z \leq 116$) from metals

By D. Wittwer[1,2,*], R. Dressler[2], R. Eichler[1,2], H. W. Gäggeler[1,2] and A. Türler[1,2]

[1] Department of Chemistry and Biochemistry, University of Bern, 3012 Bern, Switzerland
[2] Laboratory of Radiochemistry and Environmental Chemistry, Paul Scherrer Institute, 5232 Villigen, Switzerland

(Received May 23, 2012; accepted in final form September 24, 2012)
(Published online March 18, 2013)

SHE / Solid catcher / Vacuum chromatography / Diffusion

Summary. Metallic catcher foils have been investigated on their thermal release capabilities for future superheavy element studies. These catcher materials shall serve as connection between production and chemical investigation of superheavy elements (SHE) at vacuum conditions. The diffusion constants and activation energies of diffusion have been extrapolated for various catcher materials using an atomic volume based model. Release rates can now be estimated for predefined experimental conditions using the determined diffusion values. The potential release behavior of the volatile SHE Cn (E112), E113, Fl (E114), E115, and Lv (E116) from polycrystalline, metallic foils of Ni, Y, Zr, Nb, Mo, Hf, Ta, and W is predicted. Example calculations showed that Zr is the best suited material in terms of on-line release efficiency and long-term operation stability. If higher temperatures up to 2773 K are applicable, tungsten is suggested to be the material of choice for such experiments.

1. Introduction

The method of isothermal gas chromatography *e.g.* applying the on-line gas chemistry apparatus OLGA [1–4] was used to investigate the gas phase chemistry of superheavy elements (SHE) E104 (Rf), E105 (Db), E106 (Sg), and E107 (Bh). For the investigation of volatile species of Hs the cryo-thermochromatography method was developed [5]. First thermochromatographic investigations of E108 (Hs), Cn, and Fl have been performed using the Cryo On-Line Detector array [6–9]. For nuclear decay studies of several Hs isotopes the more efficient COMPACT [10, 11] was developed, which was later on also adapted for SHE adsorption studies on gold surfaces. All these methods have in common that the connection between the production of transactinide atoms in heavy ion induced nuclear fusion reactions and the setups dedicated to their chemical investigation is a stopping gas volume flushed by a carrier gas. The reaction products recoil out of the target into this volume with the momentum of the heavy ion beam particles and are there thermalized for further transport. The OLGA apparatus used a carrier gas-jet, initially saturated with aerosol particles, as transport medium for the SHE to the chemistry setup. A pure gas-jet is used for the thermochromatographic methods CTS, COLD, and COMPACT to investigate the chemical properties of volatile SHE such as Cn, E113, and Fl in their elemental state or volatile compounds such as HsO_4. The thermochromatographic methods often use a sophisticated gas-jet loop-system to transport the reaction products to the detector array. Despite specifically cleaning installations, such as hot tantalum based getters and drying cartridges, trace amounts of contaminants *e.g.* water vapor and volatile organic material enter the detector array and modify the detector surfaces in the setups, disturbing thus the measurements of correct adsorption properties. Therefore, surface monitoring with simultaneously produced chemical tracers, *e.g.* ^{185}Hg, sensitive to the contamination of the detector surfaces (gold) had to be applied [6, 7]. If required, time consuming cleaning procedures of the chromatographic surfaces during the long-term experiments had to be carried out. Stepping towards vacuum systems seems to be straightforward to circumvent these contamination problems. Another disadvantage of the gas-jet based system is the required transport time. The stopping range of the products in the gas phase [12] at ambient or elevated pressures limits the miniaturization of the recoil chambers and therefore the transport efficiency for species having half-lives shorter than 1 s. Also in these terms vacuum chromatography [13] systems seem to be a promising method for future SHE experiments. However, the lack of the gas as a thermalizing medium requires development of a suitable method to assess the recoiling nuclear reaction products at vacuum conditions. We suggest here the use of thin hot catcher foils where the recoiling products are implanted and subsequently thermally released. Because the SHE in focus have quite short half-lives in the order of single seconds or even less, the release process must be very fast. This work provides information, which materials are best suited for this task, using available diffusion and release data [14–16]. Based on Einstein's diffusion formula it can be calculated that at least diffusion coefficients of 1×10^{-8} cm^2 s^{-1} must be reached in the catcher material to provide quantitative release from 2 μm thick foils within 0.5 s. Foils of 2 μm thickness represent a good compromise between fast release and technical applicability. For ex-

*Author for correspondence (E-mail: David.Wittwer@psi.ch).

ample, a ^{238}U nucleus with 45 MeV kinetic energy will stop according to SRIM2010 within 2.6 μm (W) and 5 μm (Ti) in any metallic matrix between $21 \leq Z \leq 74$ [17]. 45 MeV kinetic energy is about the maximum recoil energy of a SHE produced in Ca induced nuclear fusion reactions. It must be considered that ions with a higher Z have shorter stopping ranges and therefore these stopping ranges represent an upper limit. Due to the variations of recoil energies from evaporation residues the number of thin foils used for stopping purposes must be adapted for every experiment separately. Besides fast release times a stable long-term operation is required accounting for the low production rates of SHE. The exploitation is strongly depending on the annealing temperature and the amount of chemically reactive trace gases in the vacuum. The ideal characteristics of a catcher foil would be to achieve as high as possible release rates at as low as possible relative temperatures θ (*i.e.* the ratio of annealing temperature to melting temperature).

In the present work we predict the diffusion constants and activation energies of SHE with $112 \leq Z \leq 116$ in the metallic host matrices Ni, Y, Zr, Nb, Mo, Hf, Ta, and W based on previously published release data for s-, d-, and p-elements from solid materials. From the predicted values release curves for the different SHE in the respective catching material are calculated, considering adsorption enthalpy predictions published in [18].

Table 1. Compilation of electron densities (n_{WS}), electro negativity factors (φ), molar volumes (V), and melting temperatures (T_M) from [16] used in the semi-empirical model of Miedema [19]. The unit d.u. (density unit) equals to 6×10^{22} electrons per cm^3 [24].

	Atomic number	$n_{WS}^{1/3}$ [d.u.]	φ [V]	$V^{2/3}$ [cm^2]	T_M [K]
Ni	28	1.75	5.20	3.52	1728
Y	39	1.21	3.20	7.34	1799
Zr	40	1.41	3.45	5.81	2128
Nb	41	1.64	4.05	4.89	2750
Mo	42	1.77	4.65	4.45	2896
Ru	44	1.83	5.40	4.06	2607
Rh	45	1.76	5.40	4.10	2237
Pd	46	1.67	5.45	4.29	1828
Hf	72	1.45	3.60	5.65	2506
Ta	73	1.63	4.05	4.89	3290
W	74	1.81	4.80	4.50	2695
Re	75	1.85	5.20	4.28	2459
Ir	77	1.83	5.55	4.17	2719
Pt	78	1.78	5.65	4.36	2041
Cn	112	1.09	3.94	5.70	
Cn[a]	112	1.14	4.0564	5.6041	
E113	113	1.05	3.85	6.85	
E114	114	1.09	4.02	6.61	
E115	115	1.12	4.09	7.68	
E116	116	1.00	4.49	7.54	

a: Values deduced from experimental data [20] (φ) and *ab-initio* calculations [25] ($V^{2/3}$).

2. Calculations

The semi-empirical model from A.R. Miedema [19] was employed to calculate enthalpies of solid solution at infinite small concentrations (ΔH_{Sol}) using a set of parameters for SHE taken from [18] (except the values from Cn* which we deduced using latest experimental adsorption data of Cn on Au [20]). Table 1 collects the used Miedema parameters which are specific for the SHE under investigation. The resulting ΔH_{Sol} together with the sublimation enthalpy (ΔH_{Subl} given in literature, *e.g.* [20–22]) yields the release enthalpy (ΔH_f), according to Eq. (1).

$$\Delta H_f = \Delta H_{Subl} - \Delta H_{Sol} \tag{1}$$

From these thermodynamic calculations the lowest release enthalpies point towards Ni, Nb, Mo, Ta, W, and Re as well suited catcher materials, see Table 2. Additionally Y, Zr, and Hf were considered due to a reported fast release of nuclear reaction products [14, 16]. The predicted release enthalpies of other metals, such as the noble metals Au, Pt, Rh, *etc.*, are comparably high, which makes theses elements thermodynamically less suited as catcher materials.

Kinetically the thermal release of single atomic species could be described as a two step process consisting of diffusion to the surface (segregation) followed by desorption. A short desorption time must be secured to calculate correct release curves from diffusion values only.

The enthalpies of adsorption, for the interesting tracer host combinations, which should be kinetically relevant to the release process of single atomic species, were calculated using the Eichler–Miedema approach from [23, 24]. They are also listed in Table 2. The accuracy of the Eichler–Miedema model is for most cases within 10% of experimentally deduced values, see *e.g.* [25, 26]. Hence, it was used to predict metallic adsorption interactions of transactinides [18]. From these values absolute adsorption enthalpies of 12 kJ/mol for Cn on Au and 94 kJ/mol for Fl on Au were derived. These values compare to experimentally deduced values of 52^{+8}_{-6} kJ/mol for Cn [6] and 34^{+54}_{-11} for Fl [7]. The Miedema model seems not to reproduce the observed trend of adsorption interactions. However, the absolute values agree within a prediction band of ±100 kJ/mol. Therefore, it can tentatively be concluded that the predicted values of absolute adsorption enthalpies from superheavy elements will most likely not differ more than ±100 kJ/mol from the real values for any tracer host combination. The confirmed experimental results for the adsorption of Cn on gold were used to deduce a new set of Miedema parameters for Cn (see Table 1). Those were used for further calculations for Cn (see Table 2). Note here, that also other theoretical calculation methods can be applied to predict absolute adsorption enthalpies on metals [27], resulting, *e.g.*, in 64 kJ/mol for Cn and 70 kJ/mol for Fl.

The mean residence time τ_a on the surface is estimated from the given adsorption enthalpies, see Table 2, using a Frenkel-like approach, Eq. (1).

$$\tau_a = \frac{1}{\nu_m} \times \exp\left(\frac{-\Delta H_{ads}}{RT}\right) \tag{2}$$

with υ_m being the maximum solid state frequency of the host material, see [28].

Indeed the mean adsorption times of SHE with $Z \geq 112$ on the surfaces of the given host materials at the high release temperatures are mostly negligible. In terms of adsorption it appears that Y retains the SHE longest from all investigated elements. In an extreme case a maximum of 1500 s

Table 2. Compilation of enthalpies of solution at infinite small concentrations (ΔH_{Sol}) and enthalpies of adsorption (ΔH_{Ads}) for SHE on different refractory metals.

	Z	Cn[a] 112	38^{+10}_{-12} kJ/mol [20]		E113 113	234 ± 14 kJ/mol [21]		Fl 114	48.6 kJ/mol [22]		E115 115	184 ± 32 kJ/mol [21]		Lv 116	146 ± 19 kJ/mol [21]	
	ΔH_{Subl}															
	Z	ΔH_{Sol} [kJ/mol]	ΔH_f [kJ/mol]	ΔH_{Ads} [kJ/mol]	ΔH_{Sol} [kJ/mol]	ΔH_f [kJ/mol]	ΔH_{Ads} [kJ/mol]	ΔH_{Sol} [kJ/mol]	ΔH_f [kJ/mol]	ΔH_{Ads} [kJ/mol]	ΔH_{Sol} [kJ/mol]	ΔH_f [kJ/mol]	ΔH_{Ads} [kJ/mol]	ΔH_{Sol} [kJ/mol]	ΔH_f [kJ/mol]	ΔH_{Ads} [kJ/mol]
Ni	28	68.75	30.75	−136.26	91.65	−142.35	−373.84	61.43	12.83	−211.62	23.64	−160.36	−420.88	265.33	119.33	−237.07
Y	39	−147.36	−185.36	−190.98	−149.88	−383.88	−394.88	−194.10	−242.70	−247.94	−266.00	−450.00	−453.85	−317.77	−463.77	−462.28
Zr	40	−101.01	−139.01	−162.00	−87.25	−321.25	−355.18	−150.14	−198.74	−224.26	−233.40	−417.40	−444.57	−221.22	−367.22	−395.36
Nb	41	87.14	49.14	−148.58	143.43	−90.57	−363.11	79.31	30.71	−209.50	30.02	−153.98	−238.57	142.48	−3.52	−321.24
Mo	42	177.04	139.04	−111.84	246.90	12.90	−330.38	198.61	150.01	−173.22	172.39	−11.61	−386.86	366.79	220.79	−231.08
Ru	44	105.21	67.21	−139.08	144.03	−89.97	−379.40	120.46	71.86	−216.62	89.79	−94.21	−432.09	371.60	225.60	−224.10
Rh	45	32.28	−5.72	−52.21	44.67	−189.33	−254.87	22.35	−26.25	−92.08	−20.86	−204.86	−282.32	246.68	100.68	−252.55
Pd	46	−58.00	−96.00	−122.93	−80.68	−314.68	−352.95	−99.78	−148.38	−186.89	−157.54	−341.54	−386.31	95.42	−50.58	−282.49
Hf	72	−66.04	−104.04	−137.20	−47.16	−281.16	−328.00	−109.32	−157.92	−196.24	−185.69	−369.69	−412.60	−152.51	−298.51	−344.44
Ta	73	78.30	40.30	−185.86	131.36	−102.64	−412.61	68.20	19.60	−257.03	17.73	−166.27	−265.64	128.12	−17.88	−381.05
W	74	201.48	163.48	−137.65	277.09	43.09	−369.44	232.96	184.36	−129.90	212.76	28.76	−437.12	429.56	283.56	−267.67
Re	75	173.87	135.87	−141.98	174.63	−59.37	−382.78	206.71	158.11	−136.69	186.42	2.42	−446.99	451.29	305.29	−248.87
Ir	77	68.15	30.15	−157.38	93.90	−140.10	−405.84	73.99	25.39	−242.69	37.62	−146.38	−243.52	335.21	189.21	−243.71
Pt	78	−8.82	−46.82	−80.39	−11.28	−245.28	−293.48	−29.05	−77.65	−126.89	−78.63	−262.63	−319.92	219.21	73.21	−223.02
Au[b]	79	135.00	97.00	−12.00				143.90	95.30	−94.00						
Au[c]	79	8.87	−29.13	−52.00	28.28	−205.72	−239.17	25.96	−22.64	−70.90	10.38	−173.62	−214.02	208.98	62.98	−146.53
Au[d]	79			−64.00						−70.00						

a: Values calculated using the experimentally deduces Miedema parameter from Table 1;
b: Miedema parameter from Ref. [18];
c: Miedema parameter from this work, see Table 1;
d: Values from Ref. [27].

is expected at temperatures of 1750 K, for the presumably strongest adsorbed Lv on Y with a maximum adsorption enthalpy of about −560 kJ/mol, including the uncertainty stated above. Therefore, this material would not be considered for experiments with Lv. The peculiarly long adsorption times on Y are already reported in [15, 29]. Generally, adsorption times of 5 ms or less are common for adsorption enthalpies of −250 kJ/mol at 1750 K.

The kinetic description of segregation is closely related to diffusion coefficients. Therefore, diffusion coefficients of transactinides in various metallic host matrices have to be

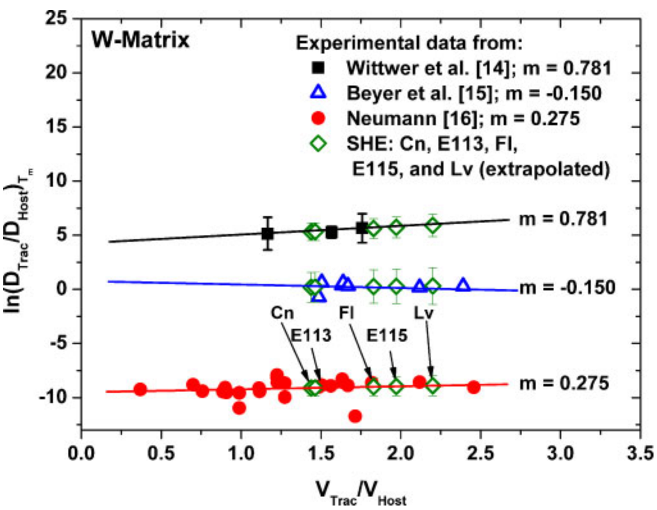

Fig. 1. The volume approach from Bakker [30] as $\ln(D_{Trac}/D_{Self})$ *vs.* $V_{Trac}/V^{\circ}_{Host}$ given for tungsten as host material at its melting temperature ($\theta = 1.00$), for details see text. The circles are data from Neumann [15], triangles from Beyer *et al.* [14], and squares from Wittwer *et al.* [16], respectively. The hollow rectangles with the error bars (1σ) are calculated values for the SHE with $112 \leq Z \leq 116$. *m*: slope of the linear regressions.

predicted from experimental results with lighter elements. The extrapolation towards SHE was made by using a volume approach introduced by Bakker [30] and further refined by Tendler and Abriata [31] postulating a linear correlation between $\ln(D_{Trac}/D_{Host})$ and $V_{Trac}/V^{\circ}_{Host}$ at a fixed relative temperature (*e.g.* $\theta = 1.00$ or $\theta = 0.95$, see Fig. 1). Here, D stands for the diffusion constants of either the tracer diffusion (D_{Trac}) in the host material or the self diffusion of the host material (D_{Host}), while V_{Trac} and V°_{Host} are the molar volumes of either the tracer (in solution) or the host material (standard state), respectively.

The volume approach can be used to predict the diffusion coefficients of SHE at certain relative temperatures if the molar volume of the SHE in the host material can be predicted. The molar volume of SHE can be deduced from quantum chemical calculation. The data published in [32–34] are used in this paper.

The individual molar volume contraction of an element in intermetallic compounds compared to its pure molar volume under standard conditions can be calculated using the expression given by Bakker [30] and Miedema and Niessen [35] for the infinitely diluted solid solution as:

$$\Delta V_{Trac} = \frac{P_0 V^{\circ\,2/3}_{Trac}\left(\varphi^*_{Trac} - \varphi^*_{Host}\right)}{\left(n^{Trac}_{WS}\right)^{-1/3} + \left(n^{Host}_{WS}\right)^{-1/3}} \times \left[\left(n^{Trac}_{WS}\right)^{-1} - \left(n^{Host}_{WS}\right)^{-1}\right] \quad (3)$$

ΔV_{Trac} is the change in molar volume of the tracer due to its dissolution in the host material. φ^*_{Trac} and φ^*_{Host} are the electronegativity parameters for the tracer and the host material, respectively and n^{Trac}_{WS} and n^{Host}_{WS} are the electron densities of the tracer and the host material at the Wigner–Seitz cell boundary. P_0 is an empirical constant derived as a best-fit parameter [19, 35, 36]. The pure molar volume of SHE under

Table 3. Collection of calculated slopes and offsets from the volume approach model as shown in Fig. 1. The T-valid is the temperature interval in which the data taken from the literature were determined. The θ indicates at which relative temperature (*i.e.* parts of the melting point) the calculations were made. The uncertainty of the slope and the offset are the 1σ uncertainties resulting from the linear regression.

		Ref. [14], Beyer *et al.*			Ref. [15], Neumann		Ref. [16], Wittwer *et al.*		
Host (T_{melt})	θ	T-valid [K]	Slope	Offset	Slope	Offset	T-valid [K]	Slope	Offset
Ni	0.95				1.19 ± 0.40	-9.61 ± 0.65	1200–1650	1.25 ± 0.43	-2.82 ± 0.79
(1728 K)	1.00				1.13 ± 0.36	-9.65 ± 0.59		1.39 ± 0.49	-3.12 ± 0.91
Y	0.95	1000–1700	-2.27 ± 0.80	0.92 ± 0.75	-2.15 ± 0.47	-0.52 ± 0.35	1350–1799		
(1799 K)	1.00		-1.96 ± 0.69	0.30 ± 0.64	-1.97 ± 0.43	-1.16 ± 0.32			
Zr	0.95	1200–2000	-2.11 ± 0.48	7.89 ± 0.57	0.72 ± 1.00	-7.15 ± 0.92	1450–2100	-0.32 ± 1.08	-4.45 ± 1.42
(2128 K)	1.00		-2.05 ± 0.53	8.27 ± 0.62	-0.29 ± 0.77	-6.43 ± 0.71		-0.22 ± 1.02	-3.83 ± 1.33
Nb	0.95	2000–2600	1.53 ± 1.46	-3.21 ± 1.78	1.07 ± 0.81	-9.44 ± 0.89	1700–2250	0.17 ± 0.60	-2.30 ± 0.86
(2750 K)	1.00		1.77 ± 1.53	-3.63 ± 1.87	0.17 ± 0.83	-8.92 ± 0.88		0.14 ± 0.54	-2.45 ± 0.78
Mo	0.95	2200–2870	0.30 ± 0.71	1.12 ± 0.97	0.11 ± 1.14	-8.71 ± 1.38	1650–2250	1.42 ± 1.14	-0.67 ± 1.27
(2896 K)	1.00		0.26 ± 0.65	0.99 ± 0.89	0.20 ± 1.09	-9.04 ± 1.31		1.39 ± 1.21	-0.85 ± 1.35
Hf	0.95	1700–2020	-0.17 ± 0.54	3.30 ± 0.78	-0.05 ± 0.47	-6.36 ± 0.67			
(2506 K)	1.00		-0.17 ± 0.57	3.32 ± 0.82	-0.08 ± 0.57	-6.32 ± 0.70			
Ta	0.95	1700–3100	0.67 ± 0.51	0.51 ± 0.85	0.17 ± 2.99	2.16 ± 2.85			
(3290 K)	1.00		0.64 ± 0.49	0.31 ± 0.82	0.15 ± 2.87	2.01 ± 2.74			
W	0.95	2400–3100	0.66 ± 0.47	-0.30 ± 0.82	0.50 ± 0.36	-9.41 ± 0.49	1350–2250	0.74 ± 0.34	4.78 ± 0.51
(3695 K)	1.00		-0.15 ± 0.60	-0.02 ± 1.08	0.28 ± 0.35	-9.51 ± 0.48		0.78 ± 0.39	4.18 ± 0.59

standard conditions is calculated as:

$$V = A/\varrho \tag{4}$$

with A the molar mass [g/mol] and ϱ the density [g/cm^3] of the SHE using *ab-initio* solid state calculations taken from [32] in the case of Cn or using Dirac–Hartree–Fock and coupled cluster calculations for E113–Lv taken from [33, 34].

Knowing V_{Host}, the volume of the tracer in solution and the self diffusion of the host material, it is possible to calculate the diffusion coefficient of any tracer at the given temperature.

The results of the linear regressions (*i.e.* the offset and slope at $\theta = 1.00$ and $\theta = 0.95$, respectively) similar to those in Fig. 1 from all investigated high-melting host materials are collected in Table 3. In principle, also lower relative temperatures of the host materials could be used for the calculations but as mentioned by Bakker in [30], the experimental data of diffusion constants and activation energies of tracer diffusion are showing a rather large spread at lower temperatures and consequently the predictive power of the correlation will be limited. This spread is getting smaller towards the melting point of an investigated material and therefore it appeared reasonable to use diffusion coefficients close to the melting points of the host material. The column T-valid in Table 3 marks the temperature interval in which the diffusion data was determined. This temperature range is particularly important regarding the Radiation Enhanced Diffusion (RED). RED was initially described by Dienes and Damsk [37] and Sizmann [38]. It increases the diffusion velocity drastically by the production of vacancies along the implantation path. The implanted tracer element can diffuse at a much higher velocity compared to the diffusion in an unaltered lattice. Therefore, higher release rates can be expected from irradiated samples. The effect was experimentally investigated several times [39–41]. A crystal lattice repairs the produced defects [38] driven by self-diffusion. This self-healing is increased at higher temperatures. Hence, the RED acceleration decreases above $\theta \sim 0.60$ [39]. The data from Wittwer *et al.* [16] and Beyer *et al.* [14] were determined using irradiated samples while the data taken from the collection of Neumann [15] were determined conventionally. As it can be seen in Fig. 1 and Table 3 this acceleration reaches up to 7 orders of magnitude in diffusion velocity. The influence of the RED effect for diffusion experiments is described in more details in [16].

Arrhenius plots of diffusion (*i.e.* a linear regression of $\ln(D)$ values plotted over $1/T$) was used to calculate diffusion constants and the activation energy of diffusion from the two diffusion coefficients deduced at $\theta = 0.95$ and $\theta = 1.00$ (for more details see [14, 16, 42]).

Subsequently, the calculation of release curves is possible using the obtained diffusion coefficients and Eq. (4), which was derived by Crank [43], Borg, and Dienes [44], assuming the independence of the release from the mean adsorption time:

$$F[\%] = 100 - \frac{800}{\pi^2} \sum_{n=0}^{\infty} \frac{1}{(2n+1)^2} \times \exp\left[-\frac{(2n+1)^2 \pi^3 Dt}{d^2}\right] \tag{5}$$

In Eq. (4) F is the released fraction [%], D the diffusion coefficient of the impurity in the host material, t the annealing time, and d the thickness of the foil.

3. Results and discussion

Figs. 2 and 3 show examples of calculated release curves using Eq. (4) and the diffusion constants and activation energies given in Table 4, which have been deduced from the values compiled in Table 3. Here, the highest possible calculated release rates are presented out of the three subsets depicted in Fig. 1 of Cn (Fig. 2), E113, Fl, E115, and Lv (Fig. 3) from different catching materials assuming 2 μm material thickness and an annealing time of 0.5 s. The re-

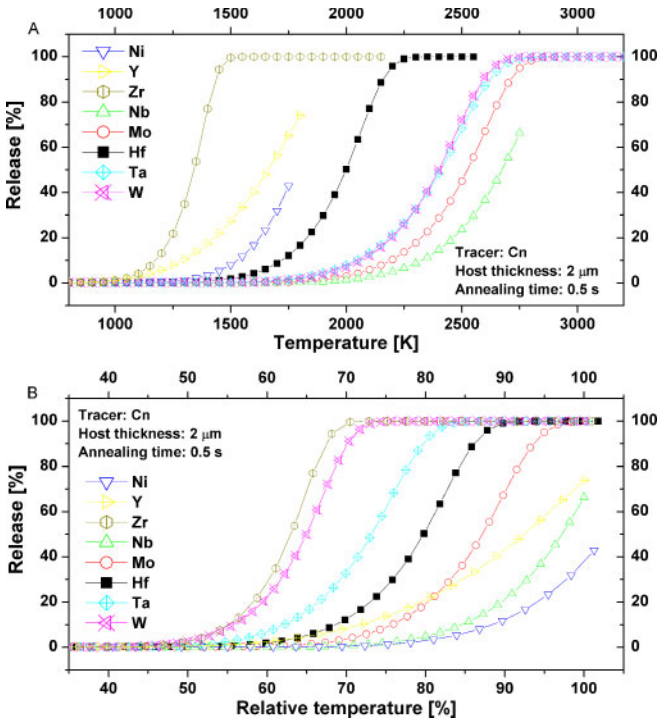

Fig. 2. (**a**) Calculated release yield of Cn out of 2 μm thick catching material at 0.5 s annealing time *vs.* the annealing temperature. The curves were calculated using the diffusion values from Table 4 and Eq. (4). (**b**) Calculated release yield of Cn *vs.* the relative temperature θ, at the same assumed experimental conditions as in (**a**).

lease curves are either based on data from [14] for Y, Zr, Nb, and Hf, from [15] for Ta, or from [16] for Ni, Mo, and W. This preselection of data has been applied to show the maximum release, which is depending on the temperature predominant during the measurements of the diffusion data and on the irradiation history of the host material. It was observed that diffusion is fastest if the annealing was performed at $\theta \sim 0.60$. The combination of thermal diffusion and RED leads to a remarkably fast diffusion. An observation of the temperature dependence of this RED effect can be seen for the diffusion values of tungsten (Table 4, and Fig. 1), where the values determined by Wittwer *et al.* [16] are much larger than those of Beyer *et al.* [14]. The annealing temperatures used for tungsten in [14] were close to the melting point. This lead to overall slower diffusion values, quite close to those measured without RED, the same can be seen for tantalum as host material in Table 3.

All calculated diffusion constants and activation energies for the different SHE atoms (tracer) and host materials are compiled in Table 4. Additionally, predictions of the 50% and 95% release temperatures after 0.5 s annealing time for each tracer/host combination are given. These values are indicative for the release characteristics of a specific tracer/host combination. Some tracers did not reach 50% or 95% release below the melting temperature of the host material. These values are marked as "not reached" (n.r.). The data reveal the expected radii dependence, meaning that generally host materials with a larger radius, such as Zr and Hf, are releasing the tracers faster on a relative temperature scale than the materials with smaller radii, such as Ni. The only exception is yttrium which has the largest radius of all investigated materials but does not reveal the highest release rates, which is in turn explainable by the high adsorption energies on this material.

The group 4 materials Zr and Hf are delivering best release at lowest possible absolute temperatures. While Zr is releasing quickly, at $\theta \sim 0.70$, Hf releases well at higher

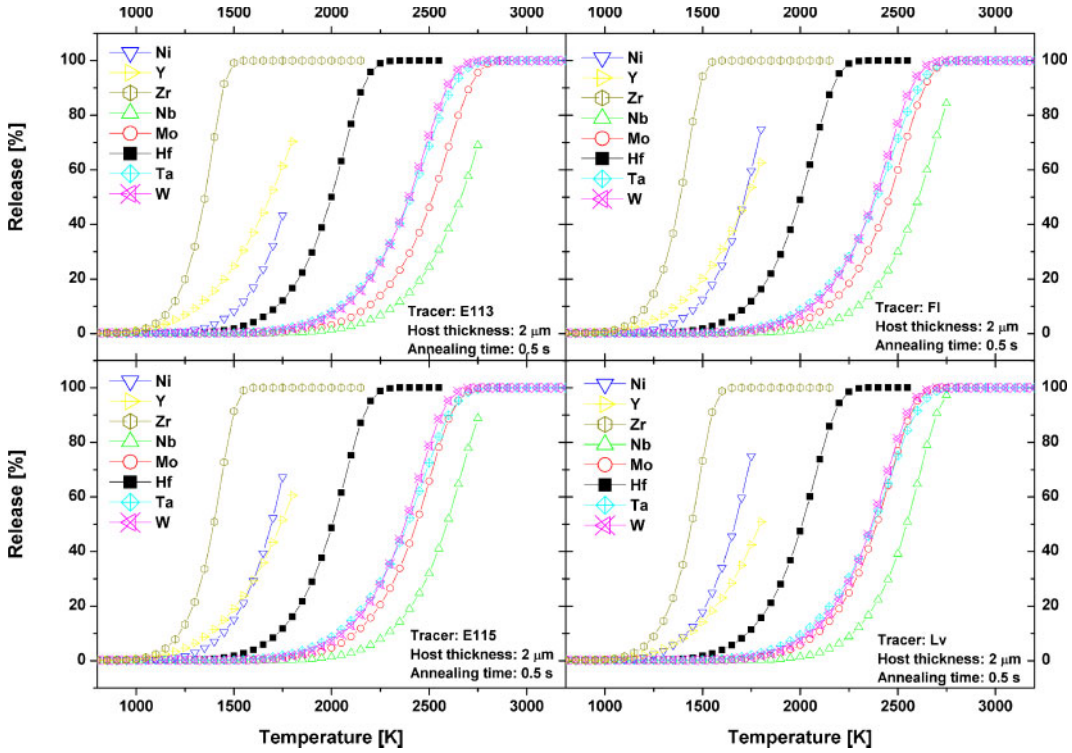

Fig. 3. Calculated release curves of the E113 (top left), Fl (top right), E115 (bottom left), and Lv (bottom right) out of 2 μm thick catching material at 0.5 s annealing time *vs.* the annealing temperature. The curves were calculated using the diffusion values from Table 4 and Eq. (4).

Table 4. Collection of diffusion constants (D_0), activation energies (E_A) and release temperatures of the 50% (T_{50}) and the 95% (T_{95}) release, respectively. The data resulted from calculations with values from Table 3.

		Ref. [14], Beyer *et al.*				Ref. [15], Neumann				Ref. [16], Wittwer *et al.*				
Ni														
T [K]										1200–1650				
Tracer	V_{Imp} [cm^3]	log D_0	E_A [kJ/mol]	T_{50} [K]	T_{95} [K]	log D_0	E_A [kJ/mol]	T_{50} [K]	T_{95} [K]	log D_0	E_A [kJ/mol]	T_{50} [K]	T_{95} [K]	Tracer
Cn	12.37					n.c.[b]	n.c.[b]			0.20	293	n.r.[a]	n.r.[a]	Cn
113	12.47					n.c.[b]	n.c.[b]			0.19	292	n.r.[a]	n.r.[a]	113
Fl	15.98					n.c.[b]	n.c.[b]			−0.12	272	1719	n.r.[a]	Fl
115	17.42					n.c.[b]	n.c.[b]			−0.24	264	1689	n.r.[a]	115
Lv	18.81					n.c.[b]	n.c.[b]			−0.36	257	1667	n.r.[a]	Lv
Y														
T [K]		1000–1700												
Tracer	V_{Imp} [cm^3]	log D_0	E_A [kJ/mol]	T_{50} [K]	T_{95} [K]	log D_0	E_A [kJ/mol]	T_{50} [K]	T_{95} [K]	log D_0	E_A [kJ/mol]	T_{50} [K]	T_{95} [K]	Tracer
Cn	17.54	−3.56	154	1667	n.r.[a]	−5.28	117	n.r.[a]	n.r.[a]					Cn
113	18.79	−3.46	160	1688	n.r.[a]	−5.25	120	n.r.[a]	n.r.[a]					113
Fl	21.45	−3.23	171	1731	n.r.[a]	−5.16	127	n.r.[a]	n.r.[a]					Fl
115	22.17	−3.17	175	1742	n.r.[a]	−5.14	129	n.r.[a]	n.r.[a]					115
Lv	25.84	−2.85	191	1796	n.r.[a]	−5.02	138	n.r.[a]	n.r.[a]					Lv
Zr														
T [K]		1200–2000								1450–2100				
Tracer	V_{Imp} [cm^3]	log D_0	E_A [kJ/mol]	T_{50} [K]	T_{95} [K]	log D_0	E_A [kJ/mol]	T_{50} [K]	T_{95} [K]	log D_0	E_A [kJ/mol]	T_{50} [K]	T_{95} [K]	Tracer
Cn	18.00	1.48	254	1343	1457	n.c.[b]	n.c.[b]			−0.41	349	n.c.[b]	n.c.[b]	Cn
113	18.90	1.45	255	1353	1474	n.c.[b]	n.c.[b]			−0.37	352	n.c.[b]	n.c.[b]	113
Fl	21.92	1.38	260	1383	1502	n.c.[b]	n.c.[b]			−0.22	359	n.c.[b]	n.c.[b]	Fl
115	22.83	1.35	261	1402	1526	n.c.[b]	n.c.[b]			−0.17	361	n.c.[b]	n.c.[b]	115
Lv	26.71	1.25	267	1446	1578	n.c.[b]	n.c.[b]			0.02	370	n.c.[b]	n.c.[b]	Lv
Nb														
T [K]		2000–2600								1700–2250				
Tracer	V_{Imp} [cm^3]	log D_0	E_A [kJ/mol]	T_{50} [K]	T_{95} [K]	log D_0	E_A [kJ/mol]	T_{50} [K]	T_{95} [K]	log D_0	E_A [kJ/mol]	T_{50} [K]	T_{95} [K]	Tracer
Cn	16.55	0.94	478	2678	n.r.[a]	n.c.[b]	n.c.[b]			−0.85	414	n.c.[b]	n.c.[b]	Cn
113	17.09	1.07	483	2666	n.r.[a]	n.c.[b]	n.c.[b]			−0.86	413	n.c.[b]	n.c.[b]	113
Fl	20.40	1.90	515	2609	n.r.[a]	n.c.[b]	n.c.[b]			−0.93	409	n.c.[b]	n.c.[b]	Fl
115	21.54	2.19	526	2596	n.r.[a]	n.c.[b]	n.c.[b]			−0.95	407	n.c.[b]	n.c.[b]	115
Lv	24.84	3.02	557	2549	2735	n.c.[b]	n.c.[b]			−1.01	403	n.c.[b]	n.c.[b]	Lv

n.r.[a] = release value not reached below the meatling temperature of the material. n.c.[b] = values not calculable, see text.

relative temperatures, see Fig. 2b. W and Ta are releasing better at lower relative temperatures compared to Hf, which would facilitate the preservation of the material to guarantee a long-term operation of the catcher foil. The sequence of release rates at given relative temperature, derived from Fig. 2b, is the same for the SHE with $112 \leq Z \leq 116$ in all investigated host materials. There are three materials Ni, Y, and Nb shown in Figs. 2 and 3, where a complete release of the tracer was not achieved below their melting temperature. Therefore these elements are not suited for future SHE experiments.

4. Conclusion

We conclude that a mixture of RED and fast thermal diffusion results in fastest release. Thus, the annealing temperature should be chosen at around 60% of the melting temperature of the catching material to assure the largest possible combined effect of thermal diffusion and increased RED. The annealing temperature may even be increased in an online in-beam experiment above 60% of the melting point, because the vacancies formed along the entrance path of the recoiling SHE are made in situ and continuously. Although, the self diffusion dependent self-healing process should be slowlier than the segregation of the vacancies.

Predictions based on the volume approach suggested by Bakker [30] were used to get first expectation data of the release characteristics of SHE from refractory, polycrystalline, metallic host materials. The extrapolation scheme presented in this work may help to predict diffusion data at various experimental conditions for any tracer from any material, where the molar volumes are known. If enough experimental data is available the calculations can be made for vacancy diffusion as well as for interstitial diffusion. Furthermore,

Table 4. Continued.

		Ref. [14], Beyer *et al.*				Ref. [15], Neumann				Ref. [16], Wittwer *et al.*				
Mo														
T [K]		2200–2870								1650–2250				
Tracer	V_{Imp} [cm^3]	log D_0	E_A [kJ/mol]	T_{50} [K]	T_{95} [K]	log D_0	E_A [kJ/mol]	T_{50} [K]	T_{95} [K]	log D_0	E_A [kJ/mol]	T_{50} [K]	T_{95} [K]	Tracer
Cn	14.31	1.11	459	2518	2741	−3.24	461	n.r.[a]	n.r.[a]	0.86	448	2527	2753	Cn
113	14.61	1.10	458	2516	2743	−3.22	463	n.r.[a]	n.r.[a]	0.88	448	2523	2748	113
Fl	18.05	1.02	451	2499	2727	−2.92	477	n.r.[a]	n.r.[a]	1.03	444	2455	2676	Fl
115	19.36	0.99	449	2496	2717	−2.80	483	n.r.[a]	n.r.[a]	1.08	442	2433	2647	115
Lv	21.76	0.94	444	2485	2703	−2.59	493	n.r.[a]	n.r.[a]	1.19	439	2388	2599	Lv
Hf														
T [K]		1700–2020												
Tracer	V_{Imp} [cm^3]	log D_0	E_A [kJ/mol]	T_{50} [K]	T_{95} [K]	log D_0	E_A [kJ/mol]	T_{50} [K]	T_{95} [K]	log D_0	E_A [kJ/mol]	T_{50} [K]	T_{95} [K]	Tracer
Cn	17.73	0.23	331	1998	2194	−3.99	326	n.r.[a]	n.r.[a]					Cn
113	18.54	0.23	331	2003	2198	−4.00	326	n.r.[a]	n.r.[a]					113
Fl	21.63	0.22	331	2005	2203	−4.05	324	n.r.[a]	n.r.[a]					Fl
115	22.60	0.21	331	2002	2199	−4.07	323	n.r.[a]	n.r.[a]					115
Lv	26.32	0.20	331	2007	2203	−4.13	321	n.r.[a]	n.r.[a]					Lv
Ta														
T [K]		1700–3100												
Tracer	V_{Imp} [cm^3]	log D_0	E_A [kJ/mol]	T_{50} [K]	T_{95} [K]	log D_0	E_A [kJ/mol]	T_{50} [K]	T_{95} [K]	log D_0	E_A [kJ/mol]	T_{50} [K]	T_{95} [K]	Tracer
Cn	16.56	−1.39	335	2493	2804	−0.56	362	2407	2674					Cn
113	17.09	−1.39	335	2488	2799	−0.56	361	2405	2672					113
Fl	20.40	−1.37	330	2457	2745	−0.61	357	2393	2651					Fl
115	21.54	−1.36	329	2436	2740	−0.63	356	2388	2648					115
Lv	24.82	−1.35	325	2401	2696	−0.67	352	2374	2637					Lv
W														
T [K]		2400–3100								1350–2250				
Tracer	V_{Imp} [cm^3]	log D_0	E_A [kJ/mol]	T_{50} [K]	T_{95} [K]	log D_0	E_A [kJ/mol]	T_{50} [K]	T_{95} [K]	log D_0	E_A [kJ/mol]	T_{50} [K]	T_{95} [K]	Tracer
Cn	13.67	−1.36	443	3282	3682	−5.24	455	n.r.[a]	n.r.[a]	0.18	394	2399	2636	Cn
113	13.91	−1.46	435	3275	3676	−5.28	451	n.r.[a]	n.r.[a]	0.19	395	2401	2639	113
Fl	17.38	−2.96	327	3146	3650	−5.93	402	n.r.[a]	n.r.[a]	0.44	403	2386	2610	Fl
115	18.74	−3.55	285	3069	3644	−6.18	383	n.r.[a]	n.r.[a]	0.53	407	2376	2597	115
Lv	20.91	−4.49	218	2908	3610	−6.59	353	n.r.[a]	n.r.[a]	0.69	412	2363	2587	Lv

n.r.[a] = release value not reached below the meatling temperature of the material. n.c.[b] = values not calculable, see text.

release rates can be determined from the obtained diffusion values even combining them with desorption data, if required.

Zr is predicted to be best suited for the efficient thermal release of SHE. Hf, as another group 4 element, is a good alternative to Zr if working at as low as possible absolute temperatures in the setup. The 50% or 95% release values of Zr and Ta are within the valid temperature range (T-valid) of the extrapolated data, see Table 3. This is not the case for W. Here the used data was investigated at lower relative temperature having therefore an increased RED effect. RED is decreasing towards higher temperature as seen in the datasets of Beyer *et al.* [14]. Therefore, the release for W as catcher material might be overestimated. The three metals Ni, Y, and Nb are not suited as catching materials.

According to the Miedema calculations, rhenium would be another valuable candidate for a fast release. Unfortunately, no self-diffusion values of this metal and therefore no extrapolations could be performed for this material.

The results gained in this work show that an efficient separation of superheavy elements through the thermal release is almost impossible. This is due to the high annealing temperatures which are mandatory to achieve high release rates. The desorption times are very short at such high temperatures, making the differences in adsorption enthalpies irrelevant in most cases. The diffusion coefficients of most elements, deduced at the same conditions (irradiated/ non irradiated host), at high relative temperatures of the host materials are very similar. Therefore, the catcher materials proposed for superheavy experiments are supposed to be best release materials for all SHE and not for any specific element.

The accuracy of the diffusion coefficients calculated with the extrapolation based on the model from Bakker is within one order of magnitude, which is a conservative value as

seen in Fig. 1. This transforms to release temperature uncertainties of ±10% for *e.g.* a 95% release.

References

1. Gäggeler, H. W., Jost, D. T., Baltensperger, U., Weber, A., Kovacs, A., Vermeulen, D., Türler, A.: OLGA II, an on-line gas chemistry apparatus for applications in heavy element research. Nucl. Instrum. Methods A **309**, 201–208 (1991).
2. Schädel, M., Brüchle, W., Dressler, R., Eichler, B., Gäggeler, H. W., Günther, R., Gregorich, K. E., Hoffman, D. C., Hübener, S., Jost, D. T., Kratz, J. V., Paulus, W., Schumann, D., Timokhin, S., Trautmann, N., Türler, A., Wirth, G., Yakuschev, A. B.: Chemical properties of element 106 (seaborgium). Nature **388**, 55–57 (1997).
3. Türler, A.: Gas phase chemistry experiments with transactinide elements. Radiochim. Acta **72**, 7–17 (1996).
4. Eichler, R., Brüchle, W., Dressler, R., Düllmann, Ch. E., Eichler, B., Gäggeler, H. W., Gregorich, K. E., Hoffman, D. C., Hübener, S., Jost, D. T., Kirbach, U. W., Laue, C. A., Lavanchy, V. M., Nitsche, H., Patin, J. B., Piguet, D., Schädel, M., Shaughnessy, D. A., Strellis, D. A., Taut, S., Tobler, L., Tsyganov, Y. S., Türler, A., Vahle, A., WiIk, P. A., Yakushev, A. B.: Chemical characterization of bohrium (element 107). Nature **407**, 63–65 (2000).
5. Kirbach, U. W., Folden, C. M., Gintera, T. N., Gregorich, K. E., Lee, D. M., Ninov, V., Omtvedt, J. P., Patin, J. B., Seward, N. K., Strellis, D. A., Sudowe, R., Türler, A., Wilk, P. A., Zielinski, P. M., Hoffman, D. C., Nitsche, H.: The cryo-thermochromatographic separator (CTS): a new rapid separation and α-detection system for on-line chemical studies of highly volatile osmium and hassium ($Z = 108$) tetroxides. Nucl. Instrum. Methods A **484**, 587–594 (2002).
6. Düllmann, Ch. E., Brüchle, W., Dressler, R., Eberhardt, K., Eichler, B., Eichler, R., Gäggeler, H. W., Ginter, T. N., Glaus, F., Gregorich, K. E., Hoffman, D. C., Jäger, E., Jost, D. T., Kirbach, U. W., Lee, D. M., Nitsche, H., Patin, J. B., Pershina, V., Piguet, D., Qin, Z., Schädel, M., Schausten, B., Schimpf, E., Schött, H.-J., Soverna, S., Sudowek, R., Thörle, P., Timokhin, S. N., Trautmann, N., Türler, A., Vahle, A., Wirth, G., Yakushev, A. B., Zielinskik, P. M.: Chemical investigation of hassium (element 108). Nature **418**, 859–862 (2002).
7. Eichler, R., Aksenov, N. V., Belozerov, A. V., Bozhikov, G. A., Chepigin, V. I., Dmitriev, S. N., Dressler, R., Gäggeler, H. W., Gorshkov, V. A., Haenssler, F., Itkis, M. G., Laube, A., Lebedev, V. Ya., Malyshev, O. N., Oganessian, Yu. Ts., Petrushkin, O. V., Piguet, D., Rasmussen, P., Shishkin, S. V., Shutov, A. V., Svirikhin, A. I., Tereshatov, E. E., Vostokin, G. K., Wegrzecki, M., Yeremin, A. V.: Chemical characterization of element 112. Nature **447**, 72–75 (2007).
8. Eichler, R., Aksenov, N. V., Albin, Y. V., Belozerov, A. V., Bozhikov, G. A., Chepigin, V. I., Dmitriev, S. N., Dressler, R., Gäggeler, H. W., Gorshkov, V. A., Henderson, R. A., Johnsen, A. M., Kenneally, J. M., Lebedev, V. Ya., Malyshev, O. N., Moody, K. J., Oganessian, Yu. Ts., Petrushkin, O. V., Piguet, D., Popeko, A. G., Rasmussen, P., Serov, A., Shaughnessy, D. A., Shishkin, S. V., Shutov, A. V., Stoyer, M. A., Stoyer, N. J., Svirikhin, A. I., Tereshatov, E. E., Vostokin, G. K., Wegrzecki, M., Wilk, P. A., Wittwer, D., Yeremin, A. V.: Indication for a volatile element 114. Radiochim. Acta **98**, 133–139 (2010).
9. Düllmann, Ch. E., Eichler, B., Eichler, R., Gäggeler, H. W., Jost, D. T., Piguet, D., Türler, A.: IVO, a device for *in situ* volatilization and on-line detection of products from heavy ion reactions. Nucl. Instrum. Methods Phys. Res. A **479**, 631–639 (2002).
10. Dvorak, J., Brüchle, W., Chelnokov, M., Dressler, R., Düllmann, Ch. E., Eberhardt, K., Gorshkov, V., Jäger, E., Krücken, R., Kuznetsov, A., Nagame, Y., Nebel1 F., Novackova, Z., Qin, Z., Schädel, M., Schausten, B., Schimpf, E., Semchenkov, A., Thörle, P., Türler, A., Wegrzecki, M., Wierczinski, B., Yakushev, A., Yeremin, A.: Doubly magic nucleus 108 $^{270}Hs_{162}$. Phys. Rev. Lett. **97**, 242501 (2006).
11. Yakushev, A. B., Türler, A.: Superheavy element 114 is a volatile metal. TAN 2011, 4th International Conference on the Chemistry and Physics of the Transactinide Elements, Sochi, Russia (2011).
12. Wittwer, D., Abdullin, F.Sh., Aksenov, N. V., Albin, Yu. V., Bozhikov, G. A., Dmitriev, S. N., Dressler, R., Eichler, R., Gäggeler, H. W., Henderson, R. A., Hübener, S., Kenneally, J. M., Lebedev, V. Ya., Lobanov, Yu. V., Moody, K. J., Oganessian, Yu. Ts., Petrushkin, O. V., Polyakov, A. N., Piguet, Rasmussen, P., Sagaidak, R. N., Serov, A., Shirokovsky, I. V., Shaughnessy, D. A., Shishkin, S. V., Sukhov, A. M., Stoyer, M. A., Stoyer, N. J., Tereshatov, E. E., Tsyganow, Yu.S., Utyonkov, V. K., Vostokin, G. K., Wegrzecki, M., Wilk, P. A.: Gas phase chemical studies of superheavy elements using the Dubna gas-filled recoil separator – Stopping range determination. Nucl. Instrum. Methods Phys. Res. B **268**, 28–35 (2010).
13. Zvara, I.: The fundamentals of vacuum thermochromatography. J. Radioanal. Nucl. Chem. **286**, 597–602 (2010).
14. Beyer, G. J., Hagebø, E., Novgorodov, A. F., Ravn, H. L., The ISOLDE collaboration. Nucl. Instrum. Methods Phys. Res. B **204**, 225–234 (2003).
15. Neumann, G.: Self Diffusion and Impurity Diffusion in Pure Metals, Pergamon Materials Series (2008).
16. Wittwer, D., Dressler, R., Eichler, R., Gäggeler, H. W., Piguet, D., Serov, A.: Thermal release studies of nuclear reaction products from polycrystalline metal matrices. Nucl. Instrum. Methods Phys. Res. B, accepted (2012).
17. Ziegler, Z. F., Ziegler, M. D., Biersack, J. P.: SRIM – The stopping and range of ions in matter. Nucl. Instrum. Methods Phys. Res. B **268** 1818–1823 (2010).
18. Eichler, B.: Metallchemie der Transaktinoide. PSI Bericht Nr. 00-09 (2000).
19. Miedema, A. R.: On the heat of formation of solid alloys II. J. Less-Common Met. **46**, 67–83 (1976).
20. Eichler, R., Aksenov, N. V., Belozerov, A. V., Bozhikov, G. A., Chepigin, V. I., Dmitriev, S. N., Dressler, R., Gäggeler, H. W., Gorshkov, V. A., Haenssler, F., Itkis, M. G., Laube, A., Lebedev, V. Ya., Malyshev, O. N., Oganessian, Yu. Ts., Petrushkin, O. V., Piguet, D., Popeko, A. G., Rasmussen, P., Shishkin, S. V., Serov, A. A., Shutov, A. V., Svirikhin, A. I., Tereshatov, E. E., Vostokin, G. K., Wegrzecki, M., Yeremin, A. V.: Thermochemical and physical properties of element 112. Angew. Chem. Int. Ed. **47**, 1–6 (2008).
21. Eichler, B.: Verflüchtigungsverhalten der Transaktinoide von Metalloberflächen uns aus Schmelzen (Thermochemische Kalkulation), PSI Bericht Nr. 03-01 (2003).
22. Hermann, A., Furthmüller, J., Gäggeler, H. W., Schwerdtfeger, P.: Spin-orbit effects in structural and electronic properties for the solid state of the group-14 elements from carbon to superheavy element 114. Phys. Rev. B **82**, 155116 (2010).
23. Eichler, B., Rossbach, H.: Adsorption of volatile metals on metal surfaces and ist application in nuclear chemistry. Radiochim. Acta **33**, 121–125 (1983).
24. Miedema, A. R.: The electronegativity parameter for transition metals: Heat of formation and charge transfer in alloys. J. Less-Common Met. **32**, 117–136 (1973).
25. Eichler, B., Buklanov, G. V., Timokhin, S. N.: Thermochromatographische Untersuchungen mit Aktinoiden in Metallkolonnen unter Vakuum. Kernenergie **30**(11/12), 469–472 (1987).
26. Gäggeler, H., Dornhöfer H, Schmidt-Ott, W. D., Greulich, N., Eichler, B.: Determination of adsorption enthalpies for polonium on surfaces of copper, silver, gold, palladium and platinum. Radiochim. Acta **38**, 103–106 (1985).
27. Pershina, V.: Relativistic electronic structure studies on the heaviest elements, Radiochim. Acta **99**, 459–476 (2011).
28. Frenkel, J.: Beitrag zur Theorie der Metalle. Z. Phys. **26**, 117–138 (1924).
29. Beyer, G. J., Novogorodov, A. F., Khalkin, V. A.: On the adsorption of ultra-micro quantities of lanthanides, Sc, Y, Zr, and Hf on polycrystalline Ta surfaces. Radiokhimya **20**, 589–597 (1978).
30. Bakker, H., Fast metal impurity diffusion in metals and the Miedema model. J. Less-Common Met. **105**, 129–138 (1985).
31. Tendler, R., Abriata, J. P.: Atomic size and fast diffusion of metallic impurities in zirconium. J. Nucl. Mater. **150**, 251–258 (1987).
32. Gaston, N., Opahle, I., Gäggeler, H. W., Schwerdtfeger, P.: Is ekamercury (element 112) a group 12 metal? Angew. Chem. Int. Ed. **46**, 1663–1666 (2007).

33. Fricke, B., Greiner, W., Waber, J. T.: The continuation of the periodic table up to $Z = 172$. The chemistry of superheavy elements, Theor. Chim. Acta **21**(3), 235–260 (1971).
34. Fricke, B.: *Structure and Bonding*. Springer-Verlag, Berlin (1975).
35. Miedema, A. R., Niessen, A. K.: Volume effects upon alloying of two transition metals. Physica B **114**, 367–374 (1982).
36. Miedema, A. R., Niessen, A. K., Buschow, K. H. J.: Some notes on diffusion in alloys containing rare earth metals. J. Less-Common Met. **100**, 71–84 (1984).
37. Dienes, G. J., Damask, A. C.: Radiation enhanced diffusion in solids. J. Appl. Phys. **29**(12), 1713–1721 (1958).
38. Sizmann, R.: The effect of radiation upon diffusion in metals. J. Nucl. Mater. **69**/**70**, 386–412 (1968).
39. Pappas, H. K., Heuser, B., Strehle, M. S.: Measurement of radiation-enhanced diffusion of La in single crystal thin film CeO_2. J. Nucl. Mater. **405**, 118–125 (2010).
40. Wittmaack, K.: Analysis of defect annealing in monocrystalline gold foils after gold ion irradiation. Phys. Stat. Solidi (b) **37**, 633–645 (1970).
41. Bonzel, H. P.: Diffusion of Ni-63 in alpha-irradiated copper. Acta Metal. **13**, 1084–1086 (1965).
42. Beyer, G. J., Novgorodov, A. F.: Zentralinstitut für Kernforschung, ZfK-317, Rossendorf (1976).
43. Crank, J.: *The Mathematics of Diffusion*. Oxford University Press, London (1975).
44. Borg, R. J., Dienes, G. J.: *An Introduction to Solid State Diffusion*. Academic Press, San Diego (1988).